IOP Publishing New J. Phys. 27 (2025) 053501 https://doi.org/10.1088/1367-2630/add558

New Journal of Physics
The open access journal at the forefront of physics

Deutsche Physikalische Gesellschaft DPG
IOP Institute of Physics

Published in partnership with: Deutsche Physikalische Gesellschaft and the Institute of Physics

OPEN ACCESS

RECEIVED
13 January 2025

REVISED
8 April 2025

ACCEPTED FOR PUBLICATION
7 May 2025

PUBLISHED
14 May 2025

PAPER

Investigation of reentrant localization transition in one-dimensional quasi-periodic lattice with long-range hopping

Pei-Jie Chang[1,*], **Qi-Bo Zeng**[2,*], **Jinghui Pi**[3,4], **Dong Ruan**[1,5] and **Gui-Lu Long**[1,5,6,7,*]

[1] State Key Laboratory of Low-Dimensional Quantum Physics and Department of Physics, Tsinghua University, Beijing 100084, People's Republic of China
[2] Department of Physics, Capital Normal University, Beijing 100048, People's Republic of China
[3] The Chinese University of Hong Kong Shenzhen Research Institute, Shenzhen 518057, People's Republic of China
[4] Department of Physics, The Chinese University of Hong Kong, Shatin, New Territories, Hong Kong Special Administrative Region of China, People's Republic of China
[5] Frontier Science Center for Quantum Information, Tsinghua University, Beijing 100084, People's Republic of China
[6] Beijing Academy of Quantum Information Sciences, Beijing 100193, People's Republic of China
[7] Beijing National Research Center for Information Science and Technology, Beijing 100084, People's Republic of China
[*] Authors to whom any correspondence should be addressed.

E-mail: cpj22@mails.tsinghua.edu.cn, zengqibo@cnu.edu.cn and gllong@tsinghua.edu.cn

Keywords: lattices, quasi-periodic disorder, reentrant localization, long-range hopping

Abstract

Reentrant localization has recently been observed in systems with quasi-periodic nearest-neighbor hopping, where the interplay between dimerized hopping and staggered disorder is identified as the driving mechanism. However, the robustness of reentrant localization in the presence of long-range hopping remains an open question. In this work, we investigate the phenomenon of reentrant localization in systems incorporating long-range hopping. Our results reveal that long-range hopping induces reentrant localization regardless of whether the disorder is staggered or uniform. We demonstrate that long-range hopping does not inherently disrupt localization; instead, under specific conditions, it facilitates the emergence of reentrant localization. Furthermore, by analyzing critical exponents, we show that the inclusion of long-range hopping modifies the critical behavior, leading to transitions that belong to distinct universality classes.

1. Introduction

Anderson localization is one of the key topics in condensed matter physics [1–3]. It refers to the suppression of wave propagation, such as electronic transport or light diffusion, in disordered media due to interference effects arising from multiple scattering. This phenomenon has been extensively studied in a variety of physical systems and has been experimentally verified in numerous works [4–25]. According to scaling theory [26], all single-particle states in one-dimensional (1D) and two-dimensional systems with uncorrelated disorder exhibit localization. In three-dimensional systems, increasing the strength of an uncorrelated disorder gives rise to a mobility edge, which defines the boundary between localized and extended states. However, in systems with correlated or structured disorder, deviations from scaling theory can occur, allowing for disorder-induced metal–insulator transitions in low-dimensional systems. The Aubry-André-Harper (AAH) model provides a framework for studying the impact of quasi-periodic disorder on localization in 1D systems [27, 28], which introduces a potential with an incommensurate period relative to the lattice sites. Due to its self-duality, the AAH model predicts that all eigenstates undergo a sharp transition from extended to localized as the system crosses the critical point, which has been confirmed in various physical realizations [4, 5, 29, 30]. Generalizations of the AAH model, such as those incorporating power-law distributed long-range hopping [31–40] or mosaic-type disorder [41–43], reveal the emergence of mobility edges in 1D systems [44–46].

Recent studies have revealed that in 1D quasi-periodic Su–Schrieffer–Heeger (SSH) systems, increasing the quasi-periodic disorder induces a reentrant localization transition [47]. Specifically, for certain dimerization strengths, some eigenstates of the system undergo a sequence of transitions: initially localized,

then delocalized, and eventually localized again as the disorder strength increases. This intriguing phenomenon has attracted significant attention [48–65]. Subsequent investigations have demonstrated that reentrant localization transitions, along with the associated mobility edges, can persist in non-Hermitian systems [49, 66–68] or systems with specific long-range hopping strengths [69]. For example, experimental studies on Si_3N_4 waveguide systems have introduced random dimer disorder, in contrast to quasi-periodic disorder, and observe analogous reentrant localization transitions [70]. Similar phenomena have also been reported in photonic crystal experimental setups [71]. Furthermore, research into the critical exponents of localization transitions has revealed a notable consistency: The critical exponents at the second and third transition points in these systems are identical, suggesting that these transitions belong to the same universality class [72]. These findings deepen our understanding of localization phenomena and the conditions under which reentrant behavior arises in various physical systems. Recent studies indicate that the presence of long-range transitions to the next-nearest neighbor disrupts the reentrant localization phenomenon. However, whether reentrant localization persists under other types of long-range transitions remains an open question for further investigation.

In this study, we investigate the 1D SSH quasi-periodic model with long-range hopping and examine localization transitions under both staggered and uniform disorder conditions. We show that the inclusion of long-range hopping not only mitigates the effect of reentrant localization, but can also induce reentrant localization under specific conditions. For staggered disorder, we observe a reentrant localization phenomenon by analyzing the phase diagram and the spatial distribution of eigenstates across lattice sites. Furthermore, the system exhibits the simultaneous presence of multiple pairs of mobility edges. A detailed analysis of the critical exponents at various phase transition points reveals that long-range hopping alters the nature of localization transitions, placing them in distinct universality classes. In the case of uniform disorder, reentrant localization and multiple pairs of mobility edges are observed within the same numerical range through phase diagram analysis. Similarly to the staggered disorder case, calculations of the critical exponents at different transition points demonstrate that long-range hopping leads to transitions belonging to different universality classes.

The remainder of the paper is organized as follows. In section 2, we provide a detailed description of the model under consideration and the computational approach used. In sections 3 and 4, we present our main findings for systems with a staggered disorder and a uniform disorder, respectively. These sections focus on the confirmation of reentrant localization and the analysis of critical exponents. In section 5, we explore the effects of inter-leg hopping on reentrant localization. Finally, a summary of our conclusions is provided in section 6.

2. Model and approach

We consider a SSH model that includes long-range hopping and incorporates either a staggered or a uniform quasi-periodic disorder term. The Hamiltonian of this model is expressed as

$$H = H_0 + H_d, \tag{1}$$

with hopping term

$$\begin{aligned} H_0 = -\sum_{i=1}^{N} \Big(& J_{11}\hat{c}_{i,A}^{\dagger}\hat{c}_{i,B} + J_1\hat{c}_{i,B}^{\dagger}\hat{c}_{i+1,A} + J_{33}\hat{c}_{i,A}^{\dagger}\hat{c}_{i+1,B} \\ & + J_3\hat{c}_{i,B}^{\dagger}\hat{c}_{i+2,A} + h.c. \Big), \end{aligned} \tag{2}$$

and the onsite quasi-periodic disorder term

$$\begin{aligned} H_d = & \sum_{i=1}^{N} \lambda_A \hat{n}_{i,A} cos\left[2\pi\beta\left(2i-1\right)+\theta\right] \\ & + \sum_{i=1}^{N} \lambda_B \hat{n}_{i,B} cos\left[2\pi\beta\left(2i\right)+\theta\right], \end{aligned} \tag{3}$$

where with $L = 2N$ representing the total number of lattice sites. Following the standard approach of the SSH model, the lattice is divided into two sublattices, A and B, with the corresponding creation and annihilation operators defined as: $\hat{c}_{i,A}^{\dagger}(\hat{c}_{i,A})$ and $\hat{c}_{i,B}^{\dagger}(\hat{c}_{i,B})$, respectively. Operators $\hat{n}_{i,A}$ and $\hat{n}_{i,B}$ represent the particle number operators for the corresponding sublattices A and B, respectively. The parameters J_1 and J_{11} denote the inter-cell and intra-cell hopping amplitudes for nearest neighbor, respectively. And J_3 and J_{33} correspond

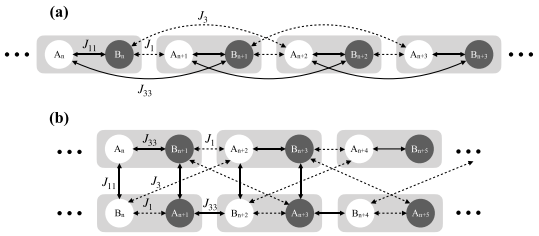

Figure 1. (a) Schematic representation of the modulated SSH model, incorporating long-range hopping terms and a quasi-periodic potential. This model consists of two sublattices, A and B. J_1, J_{11}, J_3, J_{33} represent inter-cell hopping, intra-cell hopping and the long-range hopping with different sublattices, respectively. (b) Schematic representation of the 1D model reformulated as a ladder-like structure.

to the next-nearest neighbor hopping amplitudes between different sublattices A and B as shown in figure 1(a). For convenience, we set J_1 as the unit of the energy scale throughout our study. The on-site quasi-periodic potential differs for the two sublattices: λ_A and λ_B represent the potential strengths for sublattices A and B, respectively. Without loss of generality, the quasi-periodic potential is implemented by selecting $\beta = \frac{\sqrt{7}-1}{2}$ as a Diophantine number to ensure incommensurability. We also compute cases for other irrational numbers and obtaine similar results. To minimize finite-size effects, we perform simulations on systems with sizes up to 35 422 sites. Furthermore, following standard practice in the literature and without loss of generality, we set $\theta = 0$.

We diagonalize the Hamiltonian in the single-particle lattice representation, which allows us to obtain the eigenenergy E_m and the corresponding eigenstates of equation (1) as

$$|\psi_m\rangle = \sum_{i=1}^{L} \phi_i^{(m)} |i\rangle . \tag{4}$$

Here, $\phi_i^{(m)}$ represents the probability amplitude of the corresponding m_{st} eigenstate at the i_{st} site. The localization properties of the system can be fully characterized by these eigenstates. To distinguish whether the eigenstates are localized, critical, or extended, we calculate the inverse participation ratio (IPR) and the normalized participation ratio (NPR) of the system. For the m_{th} eigenstate $\phi^{(m)}$, the definitions of the IPR and NPR are as follows:

$$\begin{aligned} \mathrm{IPR}_{(m)} &= \sum_{i=1}^{L} |\phi_i^{(m)}|^4, \\ \mathrm{NPR}_{(m)} &= \left(L \sum_{i=1}^{L} |\phi_i^{(m)}|^4 \right)^{-1}. \end{aligned} \tag{5}$$

For extended states, the IPR scales as $1/L$, approaching 0 as the system size L becomes large, while the NPR remains non-zero. For localized states, the NPR scales as $1/L$, tending to 0 as the system size L increases, while the IPR remains non-zero. For critical states, the system exhibits eigenstates where both the IPR and NPR are finite values simultaneously. To more conveniently track how the system's states evolve with varying parameters, we calculate the average IPR and NPR within a specific energy interval, defined as

$$\begin{aligned} \mathrm{IPR} &= \frac{1}{m} \sum_{m} \mathrm{IPR}_{(m)}, \\ \mathrm{NPR} &= \frac{1}{m} \sum_{m} \mathrm{NPR}_{(m)}. \end{aligned} \tag{6}$$

For the subsequent analysis of the critical exponents, we define the mean square NPR as

$$\sigma = \sqrt{\mathrm{NPR}}. \tag{7}$$

Near the phase transition critical point, the critical behavior of a parameter can be described by the following power law:

$$\sigma \sim (-\varepsilon)^{\beta}, \; L * \mathrm{NPR} \sim \varepsilon^{-\gamma}, \; \xi \sim |\varepsilon|^{-\nu}. \tag{8}$$

Here, $\varepsilon = (\lambda - \lambda_c)/\lambda_c$ with λ_c is the critical quasi-periodic disorder strength for the localization transition, and ξ represents the correlation length. According to [72, 73], we can calculate the R function for systems of different sizes

$$R[L, L'] = \frac{\ln\left(\sigma_L^2/\sigma_{L'}^2\right)}{\ln\left(L/L'\right)} + 1. \tag{9}$$

The curves intersect at a single common point at the localization transition for different system sizes L and L'. The horizontal coordinate of the intersection point corresponds to the strength of the critical disorder λ_c, while the vertical coordinate gives the ratio of the critical exponents γ/ν. Near the localization transition point, systems of different size L follow the same scaling function G as

$$\sigma^2 = L^{\gamma/\nu - 1} G\left(\varepsilon L^{1/\nu}\right). \tag{10}$$

Through this relationship, the critical exponent ν can be determined by minimizing the relative error of the scaling function G, which allows the analysis of critical properties near different critical points of the localization transition.

As shown in [47], it is found that under staggered disorder, defined as $\lambda_A = -\lambda_B$, the system exhibits a reentrant localization transition. Calculations of the critical exponents indicate that the second and third transitions belong to the same universality class. In contrast, no reentrant localization transition is observed under uniform disorder, defined as $\lambda_A = \lambda_B$. However, in systems with long-range hopping, both staggered disorder and uniform disorder display reentrant localization features in the phase diagram, with critical exponents differing from those observed in systems without long-range hopping.

In the next section, we focus on discussing the influence of long-range hopping under staggered disorder and uniform disorder separately. To better characterize the localization transitions between the critical state and other states, we define quantity η consistent with [47, 74] as follows:

$$\eta = \log_{10}\left(\mathrm{IPR} \times \mathrm{NPR}\right), \tag{11}$$

where IPR and NPR are taken the average over all the eigenstates as shown in equation (6). When both $\langle \mathrm{IPR} \rangle$ and $\langle \mathrm{NPR} \rangle$ are finite ($\sim \mathcal{O}(1)$) we have $\eta \in [-2, -1]$. However, when the system is entirely in local states or extended states, we have $\mathrm{IPR} \times \mathrm{NPR} \sim L^{-1}$. The system sizes we typically simulate are above 1000, and in this case, the obtained η will be less than -3. As a result, a smaller value of η corresponds to an extended or localized state, while a higher value of η indicates a critical state.

3. Staggered disorder

Previous literature [47] has discussed the occurrence of a reentrant localization transition under staggered disorder. When long-range next-nearest neighbor hopping is simply added to the model with the same parameters, it is observed that the reentrant localization transition gradually weakens and eventually disappears, as shown in figure 2. Specifically, for $L = 3194$, $J_3 = 0$ and for varying $J_{33} = 0, 0.1, 0.3, 0.5$, the reentrant localization transition essentially disappears when J_{33} reaches approximately 0.3. This result is consistent with the findings in [69], where the introduction of long-range hopping between the same lattice sites in different unit cells weakens the formation of dimers. As a result, the competition between the dimers and disorder diminishes, ultimately preventing the transition from localized to extended states.

However, describing long-range hopping as merely weakening the reentrant localization transition is not entirely accurate. When the system is tuned to the appropriate parameters, such as $J_{11} = J_3 = 0.1$, the reentrant localization transition still appears in the η phase diagram for the same system size, as clearly demonstrated in figure 3. We should point out that this observation does not completely contradict the previous conclusions of [69]. In the presence of long-range hopping, the originally 1D chain-like system can be effectively reduced to a 1D ladder structure, as shown in figure 1(b). In this ladder configuration, the emergence of reentrant localization can be understood as a competition between dimers and disorder terms in each leg, similar to the 1D chain, leading to the reentrant localization transition. Therefore, even with long-range hopping, the characteristic of reentrant localization can still arise under conditions of small inter-leg hopping.

Moreover, the behavior of the reentrant localization in this case is not directly related to the topological phase transition of the system. As shown in figure 3, the reentrant localization feature begins to emerge when $J_{33}/J_1 > 2.3$. In the presence of long-range hopping, the SSH model exhibits a multi-phase diagram, with the phase transition occurring near $J_{33} = J_1$ [75, 76]. This suggests that the emergence of reentrant localization is not a result of the topological phase transition even with long-range hopping.

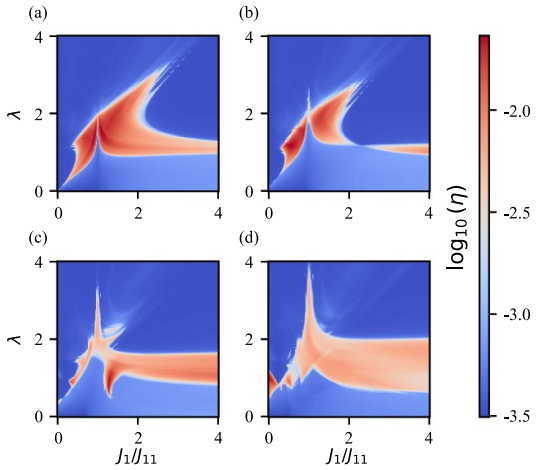

Figure 2. η phase diagrams of the system in λ and J_1/J_{11} plane with $J_3 = 0$ and $\beta = \frac{\sqrt{5}-1}{2}$ for (a) $J_{33} = 0$, (b) $J_{33} = 0.1$, (c) $J_{33} = 0.3$, (d) $J_{33} = 0.5$, where the system size $L = 3194$ and $\lambda_A = -\lambda_B$. The color represents different values of $\log_{10}(\eta)$. And the red region corresponds to the intermediate states where single-particle mobility edges exist, while the blue region indicates that the system is entirely in the localized or extended state.

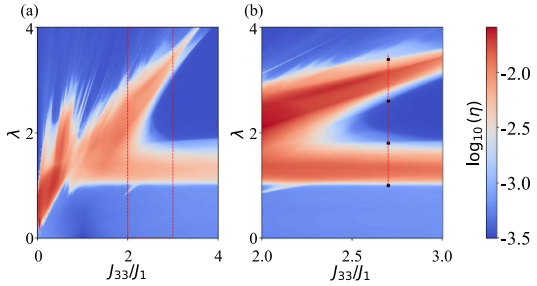

Figure 3. η phase diagrams of the system in λ and J_{33}/J_1 plane with $J_{11} = J_3 = 0.1$, the system size $L = 3194$ and $\lambda_A = -\lambda_B$. The color represents different values of $\log_{10}(\eta)$. (b) A zoomed-in version of the portion enclosed by the dashed box in (a). The dashed line in (b) is located at $J_{33}/J_1 = 2.7$, and the black dots represent schematic localization transition points.

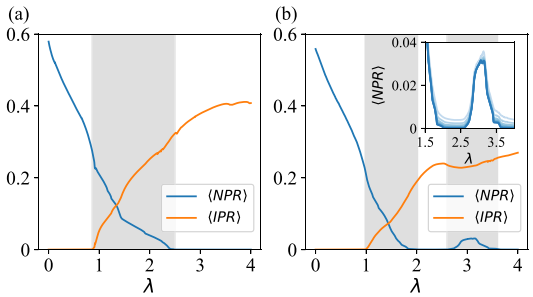

Figure 4. (a) and (b) Show the average IPR and NPR over all eigenstates for $J_{33}/J_1 = 0.5$ and $J_{33}/J_1 = 2.7$, respectively, for the case of staggered disorder and system size $L = 13530$. The shaded regions represent the critical area, where both localized and extended states coexist. The inset in (b) displays the average NPR for $L = 1220, 1974, 3194, 5168, 8362, 13\,530, 21\,892$, and $35\,422$, with the color intensity ranging from light to dark.

In figures 4(a) and (b), we present the average IPR and NPR over all eigenstates for two different cases, $J_{33}/J_1 = 0.5$ and $J_{33}/J_1 = 2.7$, marked by the dotted line in figure 3(b). As shown in figure 4(a) for $J_{33}/J_1 = 0.5$, a critical region appears when $0.86 < \lambda < 2.5$. After the localization transition, for $\lambda > 2.5$, all eigenstates of the system remain localized, and no further extended states appear as λ increases. In contrast, for $J_{33}/J_1 = 2.7$ in figure 4(b), two critical regions are observed: $0.98 < \lambda < 2.018$ and $2.599 < \lambda < 3.6$, where both IPR and NPR take finite values. Between these two critical regions and beyond the second critical region, all eigenstates exhibit localized characteristics. It is noteworthy that the second critical region is much smaller than the first. To rule out the possibility of finite-size effect, we calculate the results for different system sizes: $L = 1220, 1974, 3194, 5168, 8362, 13\,530, 21\,892, 35\,422$. In the inset of figure 4(b), we observe

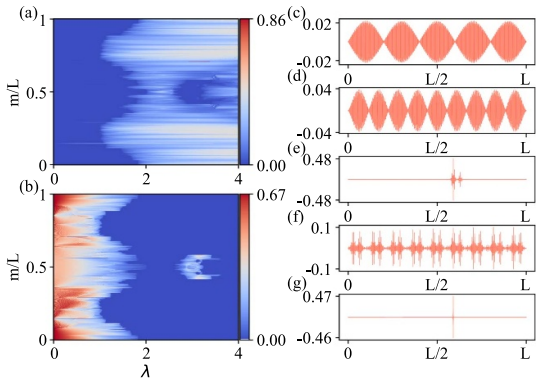

Figure 5. (a) The IPR and (b) NPR associated with the eigenstate indices as a function of λ for $J_{33}/J_1 = 2.7$, respectively. (c)–(g) illustrate the spatial distribution of eigenstates across lattice sites for $\lambda = 0.4, 1.2, 2.1, 2.7, 4$, with eigenstate index $m/L = 0.5$ and $L = 13\,530$.

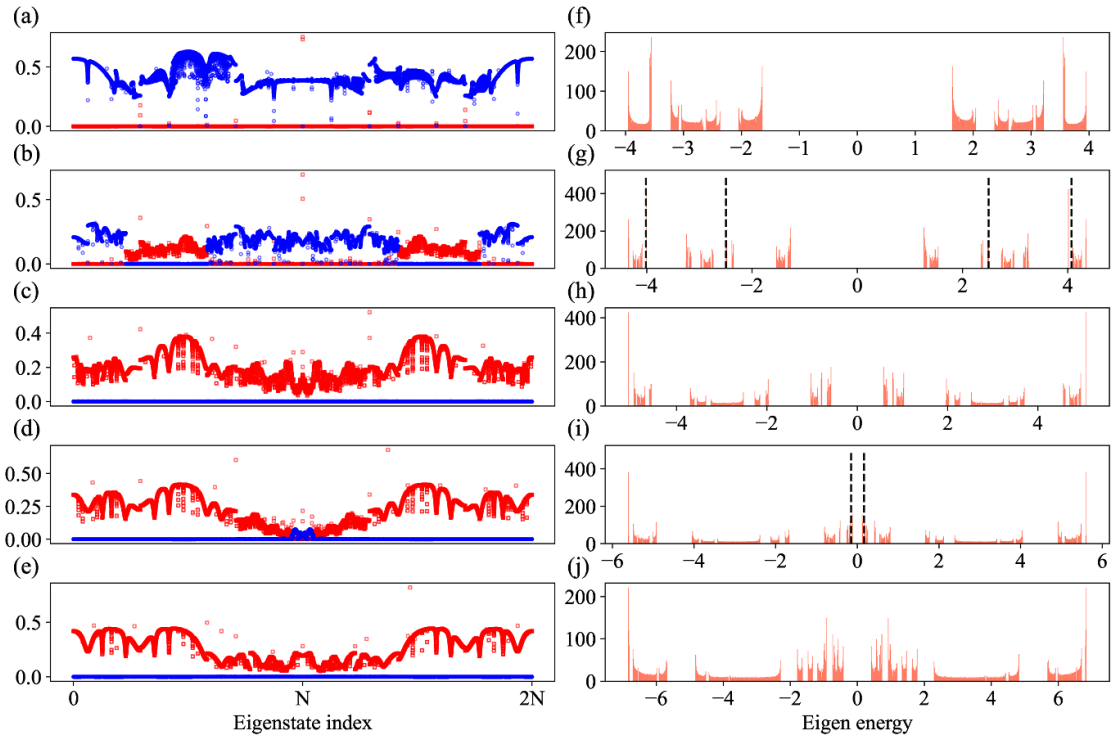

Figure 6. (a)–(e) Show the distributions of IPR (red) and NPR (blue) as functions of the eigenstate index for $\lambda = 0.4, 1.2, 2.1, 2.7$ and 4, respectively. (f)–(j) Display the density of states (DOS) as a function of eigenenergy for the same λ values, with the black dashed lines indicating the locations of single-particle mobility edges.

that as the size of the system L increases, the second critical region persists, indicating the stability of the reentrant localization feature in the staggered system with long-range hopping.

To better understand which eigenstates undergo reentrant localization transitions as the disorder strength λ changes, we fix $J_{33}/J_1 = 2.7$ and plot colormaps of the IPR and NPR as functions of the eigenstate energy ordered index and λ in figure 5. The colormaps reveal that some eigenstates in the central energy range transition from localized to extended states in the range $2.6 < \lambda < 3.6$. Furthermore, we plot the spatial distribution of the eigenstate with $m/L = 0.5$ for $\lambda = 0.4, 1.2, 2.1, 2.7$ and 4. It is evident that the eigenstate is clearly localized at $\lambda = 2.1$, but as λ increases to 2.7, the eigenstate transitions to an extended state.

The colormaps demonstrate the presence of single-particle mobility edges in this 1D system. To more clearly identify the locations of the mobility edges, we show the distributions of IPR and NPR as functions of the eigenstate index for $\lambda = 0.4, 1.2, 2.1, 2.7, 4$ in figures 6(a)–(e). From figure 6, we observe that as λ increases, single-particle mobility edges appear at $\lambda = 1.2$. These mobility edges then vanish, only to reemerge as λ continues to increase. At higher values of λ, the mobility edges eventually disappear

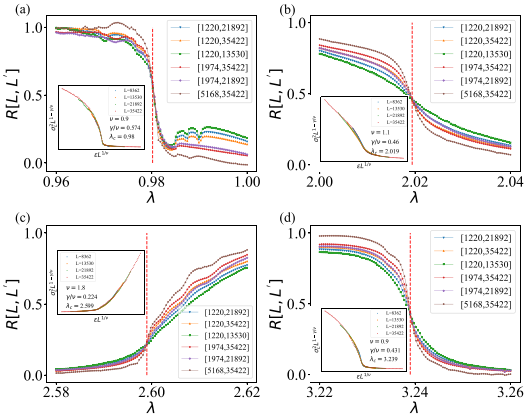

Figure 7. (a)–(d) Depict the values of the function $R[L,\ L']$ near the first, second, third, and fourth critical quasi-periodic disorder potential strength, with $J_{33}/J_1 = 2.7$ and $\lambda_A = -\lambda_B$. In each panel, the inset presents the σ^2 of the fitted critical exponent ν near the respective critical quasi-periodic disorder strength. The coordinate of the function $R[L,\ L']$ crossing point is denoted as $(\lambda_c, \gamma/\nu)$. For the first critical point, we average the NPR of eigenstates with $m/L \in [0.238, 0.243]$. For the second, third, and fourth critical points, we average the NPR of eigenstates with $m/L \in [0.48, 0.52]$.

completely. Similarly, the presence of single-particle mobility edges is also evident in the system's density of states (DOS), as shown in figures 6(f)–(j).

It is noteworthy that in figure 6(b), the system first exhibits single-particle mobility edges, with two pairs of mobility edges observed. This behavior contrasts with those of systems lacking long-range hopping, where typically only one pair of single-particle mobility edges is present. Correspondingly, the DOS in figure 6(g) also displays symmetric two pairs of mobility edges. We interpret this as follows: In systems with long-range hopping, the structure can be viewed as a 1D ladder system. When there is no coupling between the two legs of the ladder (that is, $J_{11} = J_3 = 0$), each leg can independently exhibit one pair of mobility edges. However, due to the difference in parameters between the two legs, the positions of the mobility edges will also differ. When $J_{11} \neq 0$ and $J_3 \neq 0$, the coupling acts as a perturbation that may shift the positions of the mobility edges. Nevertheless, the system retains two pairs of mobility edges. In a word that long-range hopping introduces additional pairs of mobility edges into the system, providing greater flexibility for studying the critical states in 1D systems.

Furthermore, we investigate the critical behavior at various localization transition points. By zooming in figures 5(a) and (b), we preliminarily identify the critical disorder strengths, λ_c, associated with the localization transitions. In a narrow region around each λ_c, we calculate the $R[L, L']$ function based on equation (9). In figure 7, we present the $R[L, L']$ functions for different localization transition points. The crossing points of these $R[L, L']$ functions on the horizontal axis determine the strengths of critical disorder, λ_c, for the four localization transitions indicated by the black dots in figure 3(b). The corresponding strengths of critical disorder for each transition are as follows: $\lambda_{c,1} = 0.9802$, $\lambda_{c,2} = 2.0194$, $\lambda_{c,3} = 2.599$, and $\lambda_{c,4} = 3.239$. The vertical coordinates of the crossing points correspond to the critical exponent ratio γ/ν for the four transition points, which are given by $\gamma_1/\nu_1 = 0.57 \pm 0.016$, $\gamma_2/\nu_2 = 0.46 \pm 0.006$, $\gamma_3/\nu_3 = 0.22 \pm 0.007$, and $\gamma_4/\nu_4 = 0.43 \pm 0.009$. Following the description in equation (10), we plot $\sigma^2 L^{1-\gamma/\nu}$ and $\varepsilon L^{1/\nu}$ as functions of system size, with $L = 8362, 13\,530, 21\,892$ and $35\,422$. Adjusting the critical exponent ν, we align the $\sigma^2 L^{1-\gamma/\nu}$ and $\varepsilon L^{1/\nu}$ curves for different L, achieving optimal overlap. This approach provides an optimal estimate for the critical exponent ν. The calculated values of ν for the four localization transitions are $\nu_1 = 0.9$, $\nu_2 = 1.1$, $\nu_3 = 1.8$ and $\nu_4 = 0.9$.

In contrast to the results obtained for systems without long-range hopping [72], our calculated critical exponents ν indicate that the second and third localization transition points in the model with long-range hopping do not belong to the same universality class. While the critical exponents ν for the first and fourth localization transition points are identical, their values γ/ν differ, suggesting that the γ values at these two localization transition points are distinct. This implies that, in the presence of long-range hopping, the critical behaviors at the four localization transition points belong to different universality classes.

Furthermore, we calculate the critical exponents corresponding to different localization transition points using the scaling law for $\mathrm{NPR}_L * L$. According to equation (8), we know that $\mathrm{NPR}_L * L \sim L^{\gamma/\nu}$. By fitting the linear relationship between $\log(L)$ and $\log(\mathrm{NPR}_L * L)$ using the least-squares method, we determine the critical exponent ratio γ/ν as shown in figure 8. The fitting yields the following critical exponent ratios for the four localization transition points: $\gamma_1/\nu_1 = 0.5735 \pm 8 \times 10^{-05}$, $\gamma_2/\nu_2 = 0.4607 \pm 1.4 \times 10^{-04}$, $\gamma_3/\nu_3 = 0.2243 \pm 2.3 \times 10^{-05}$ and $\gamma_4/\nu_4 = 0.4309 \pm 1 \times 10^{-04}$. These results are consistent with those

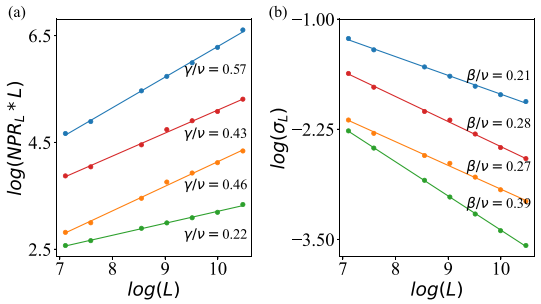

Figure 8. The critical exponent ratio (a) γ/ν and (b) γ/β for the four critical quasi-potential points. These ratios are obtained by fitting $\log(\mathrm{NPR}_L * L)$ against $\log(L)$. The system sizes L used for the fitting are: 1220, 1974, 5168, 8362, 13 530, 21 892, and 35 422.

obtained previously from the vertical coordinates of the $R[L, L']$ function. Furthermore, from equation (8), we also know that $\sigma_L \sim L^{-\beta/\nu}$. Similarly, by applying the least squares method to fit the linear relationship between $\log(L)$ and $\log(\sigma_L)$, we determine the corresponding critical exponent β/ν for the four localization transition points as follows: $\beta_1/\nu_1 = 0.2133 \pm 2 \times 10^{-05}$, $\beta_2/\nu_2 = 0.2696 \pm 3.5 \times 10^{-05}$, $\beta_3/\nu_3 = 0.3879 \pm 6 \times 10^{-06}$, and $\beta_4/\nu_4 = 0.2846 \pm 2.6 \times 10^{-05}$. The critical exponents we obtained should satisfy the hyperscaling law [73] as

$$\frac{2\beta}{\nu} + \frac{\gamma}{\nu} = 1. \tag{12}$$

We confirm that the critical exponents obtained in this study satisfy the hyperscaling relation.

4. Uniform disorder

Previous studies have shown that reentrant localization transitions occur exclusively in 1D systems with staggered disorder or with a large detuning between intra-cell and inter-cell hopping in the presence of uniform disorder [65]. In contrast, for 1D systems with uniform disorder and small detuning between intra-cell and inter-cell hopping, only single-particle mobility edges have been reported. In this work, we investigate the localization properties of a 1D system with uniform disorder in the presence of long-range hopping. Our results reveal that, when long-range hopping is introduced, the system exhibits reentrant localization transitions, a phenomenon that was previously not observed in uniform disorder systems without long-range hopping under small detuning.

Initially, we consider the case where $J_{11} = J_3 = 0$. In this scenario, the system can be treated as a 1D ladder model with no coupling between the two legs of the ladder. Under these conditions, we calculate the system's η-phase diagram, as shown in figure 9(a). The diagram clearly reveals a critical transition region, indicating that as the disorder strength increases, the system transitions from an extended state to a regime where some eigenstates become localized. At this stage, the system exhibits single-particle mobility edges. As the strength of the disorder is further increased, the system eventually fully transitions into a localized state. These observations are consistent with previous studies on systems with uniform disorder.

Next, we introduce coupling between the two legs of the ladder structure by setting the inter-leg hopping parameters to $J_{11} = J_3 = 0.1$. Under these conditions, we recalculate the η-phase diagram. Compared to figure 9(a), the updated phase diagram reveals additional spike-like structures, highlighted by the dashed box in figure 9(b). To investigate this further, we zoom in on the region within the dashed box, as shown in figure 9(c). In this magnified view, we observe that at one of the spikes, as the disorder strength λ increases, the system transitions from an extended state to a critical state and eventually to a fully localized state. Notably, as λ continues to increase, some localized eigenstates revert to extended states within the spike. Eventually, when λ becomes sufficiently large, all eigenstates become fully localized.

We select the parameter $J_{33}/J_1 = 0.7$, as shown in figure 9(c), and calculate distributions of the IPR and NPR of the system as functions of disorder strength λ and the eigenstate index. Figures 10(a) and (b) show that, as λ increases, most eigenstates transition from extended to localized states. However, for eigenstates near the lowest and highest eigenenergy, a reentrant localization transition occurs. To further illustrate this phenomenon, figures 10(c)–(g) depict the spatial distribution of a specific eigenstate indexed by $m/L = 0$ for λ values of 0.4, 1.2, 2.2, 2.41, and 4, respectively. At $\lambda = 2.2$, the eigenstate transitions into a localized state. As λ increases to 2.41, the eigenstate reverts to an extended state, before localizing again as λ increases further. Notably, comparing the delocalization observed here (figure 10(f)) with that observed under

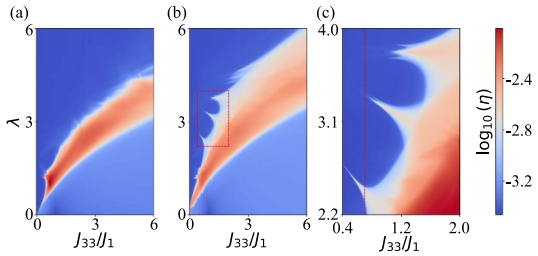

Figure 9. η phase diagrams of the system in λ and J_{33}/J_1 plane with (a) $J_{11} = J_3 = 0$, (b) $J_{11} = J_3 = 0.1$, the system size $L = 3194$ and $\lambda_A = \lambda_B$. (c) The zoomed-in version of the portion enclosed by the dashed box in (b). The color represents different values of $\log_{10}(\eta)$. The dashed line in (c) is located at $J_{33}/J_1 = 0.7$.

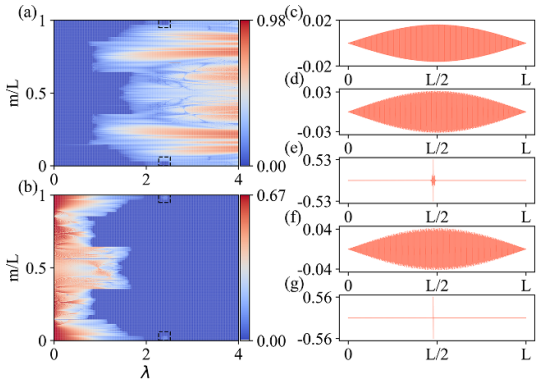

Figure 10. (a) The IPR and (b) NPR associated with the eigenstate indices as a function λ for $J_{33}/J_1 = 0.7$, respectively. The position marked by the dotted line corresponds to the reentrant localization point. (c) to (g) illustrate the spatial distribution of eigenstates across lattice sites for $\lambda = 0.4, 1.2, 2.2, 2.41, 4$, with eigenstate index $m/L = 0$ and $L = 13\,530$.

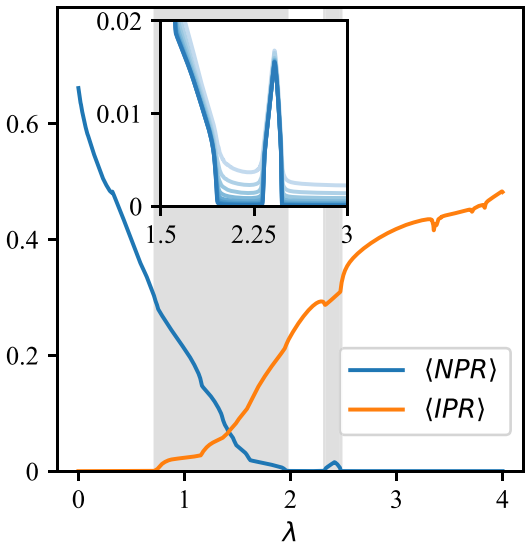

Figure 11. The average IPR and NPR over eigenstates with $m/L \in [0, 1/6]$ for $J_{33}/J_1 = 0.7$, for the case of uniform disorder and system size $L = 13\,530$. The shaded regions represent the critical area, where both localized and extended states coexist. The inset shows the average NPR for $L = 1220, 1974, 3194, 5168, 8362, 13\,530, 21\,892$, and $35\,422$ with the color intensity ranging from light to dark.

staggered disorder conditions (figure 5(f)), we find that the eigenstates in figure 10(f) exhibit a more extended spatial distribution.

To rule out the finite-size effects, we calculate the average IPR and NPR over eigenstates with $m/L \in [0, 1/6]$ as functions of disorder strength λ, and plot the results in figure 11. In the second shaded region, a characteristic feature of reentrant localization emerges. The inset of figure 11 provides a magnified view of this region, showing the results for different system sizes:

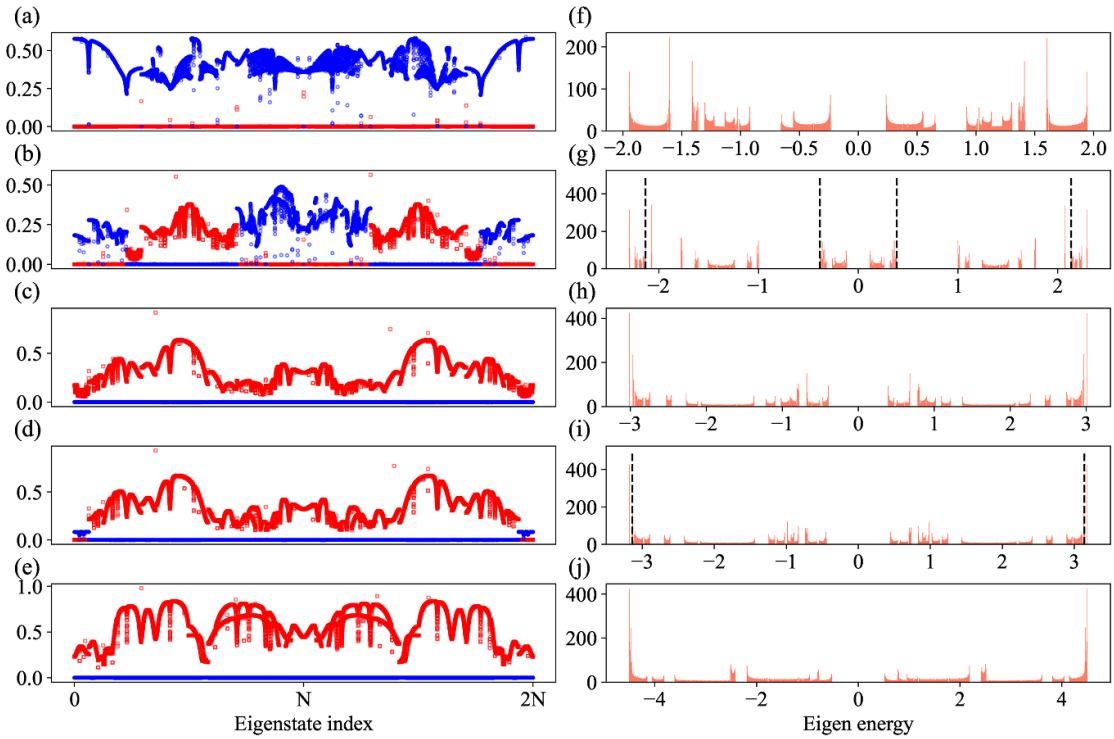

Figure 12. (a)–(e) Show the distributions of IPR (red) and NPR (blue) as functions of the eigenstate index for $\lambda = 0.4$, 1.2, 2.2, 2.41 and 4, respectively. (f)–(j) Display the DOS as a function of eigenenergy for the same λ values, with the black dashed lines indicating the locations of single-particle mobility edges.

$L = 1220, 1974, 3194, 5168, 8362, 13\,530, 21\,892$, and $35\,422$ with colors ranging from light to dark. For all system sizes, the reentrant localization feature persists, confirming that the observed localization transition is not influenced by finite-size effects.

To further explore how the mobility edges evolve with increasing disorder strength λ, we plot the distributions of IPR and NPR as functions of the eigenstate index in figures 12(a)–(e) for $\lambda = 0.4$, 1.2, 2.2, 2.41 and 4, respectively. At $\lambda = 0.4$ (figure 12(b)), the system exhibits mobility edges, which appear in pairs and separate localized and extended states within the spectrum, indicating the coexistence of both the extended state and the localized state of eigenstates. As λ increases to 2.2 (figure 12(c)), the mobility edges disappear, and all eigenstates become localized, signaling a complete transition to a fully localized phase. Interestingly, at $\lambda = 2.4$ (figure 12(d)), a subset of eigenstates transitions back to extended states, leading to the reappearance of mobility edges. In this case, the extended states are located near the highest and lowest eigenenergy, in contrast to the staggered disorder scenario, where the extended states typically emerge in the middle of the eigenenergy spectrum. Finally, as λ increases further to 4 (figure 12(e)), all eigenstates become localized again. The corresponding DOS plots are shown in figures 12(f)–(j), which clearly reflect the changes in the mobility edges as λ varies. The appearance, disappearance, and reappearance of extended states align with the observations from the IPR and NPR distributions.

In figure 13, we calculate the critical exponents at different localization transition points. Using the parameters marked by the dashed line in figure 9(c), specifically $J_{33}/J_1 = 0.7$, we evaluate the R-function in a small neighborhood around the critical disorder strengths λ_c. As discussed previously, the horizontal coordinate of the intersection points of the R-function provides the critical disorder strength λ_c for each localization transition, while the vertical coordinate corresponds to the ratio of critical exponents γ/ν. From the analysis of the R-function results in figure 13, we determine the critical disorder strengths for the four localization transitions as $\lambda_{c,1} = 0.7634$, $\lambda_{c,2} = 1.9502$, $\lambda_{c,3} = 2.3210$ and $\lambda_{c,4} = 2.4726$, with the corresponding critical exponent ratios $\gamma_1/\nu_1 = 0.4849 \pm 0.0092$, $\gamma_2/\nu_2 = 0.5088 \pm 0.0113$, $\gamma_3/\nu_3 = 0.3771 \pm 0.012$ and $\gamma_4/\nu_4 = 0.3645 \pm 0.0221$. Based on the description of equation (10), we plot the relationship $\sigma^2 L^{1-\gamma/\nu}(\varepsilon L^{1/\nu})$ in the insets of figure 13. For systems of different sizes, the equation should follow the same functional relationship when calculated using the optimally fitted ν. Accordingly, we perform calculations for four systems with sizes $L = 8362, 13\,530, 21\,892$ and $35\,422$. The fitting process yields the following optimal critical exponents: $\nu_1 = 0.814$, $\nu_2 = 1.10$, $\nu_3 = 0.938$, and $\nu_4 = 0.680$. These results are consistent with those obtained for the staggered disorder system, confirming that each of the four localization transition points exhibits distinct critical exponents.

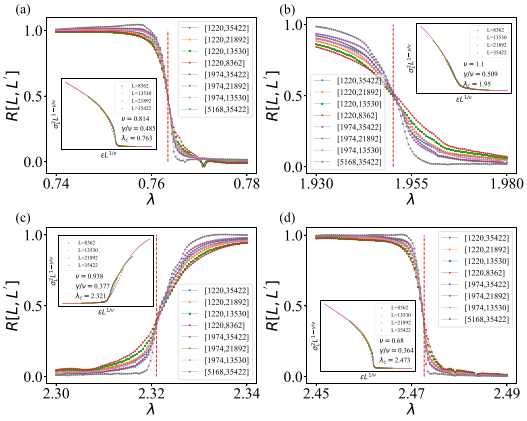

Figure 13. (a)–(d) Depict the values of the function $R[L,\ L']$ near the first, second, third, and fourth critical quasi-periodic disorder potential strength, with $J_{33}/J_1 = 0.7$ and $\lambda_A = \lambda_B$. In each panel, the inset presents the σ^2 of the best fitted critical exponent ν near the respective critical quasi-periodic disorder potential strength. The coordinates of the function $R[L,\ L']$ crossing point is denoted as $(\lambda_c, \gamma/\nu)$. For the first critical point, we average the NPR of eigenstates with $m/L \in [0.167, 0.177]$. For the second, third, and fourth critical points, we average the NPR of eigenstates with $m/L \in [0, 0.1]$.

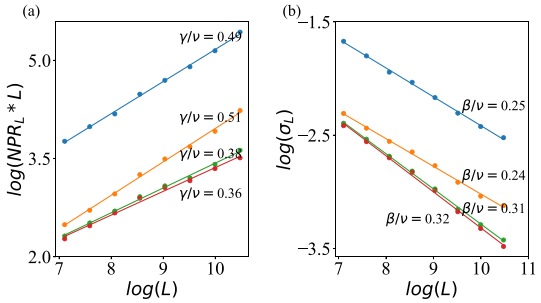

Figure 14. The critical exponent ratio (a) γ/ν and (b) γ/β for the four critical quasi-potential points. These ratios are obtained by fitting $\log(\mathrm{NPR}_L * L)$ against $\log(L)$. The system sizes L used for the fitting were: 1220, 1974, 5168, 8362, 13 530, 21 892, and 35 422.

Similarly, we can use the scaling law of $\mathrm{NPR}_L * L$ to fit the critical exponents, as shown in figure 14. According to equation (8), by fitting the slope of $\log(L)$ and $\log(\mathrm{NPR}_L * L)$, we obtain the critical exponent ratios γ/ν at the four localization transition points: $\gamma_1/\nu_1 = 0.4907 \pm 7.6 \times 10^{-05}$, $\gamma_2/\nu_2 = 0.5106 \pm 1 \times 10^{-04}$, $\gamma_3/\nu_3 = 0.3792 \pm 7 \times 10^{-05}$ and $\gamma_4/\nu_4 = 0.3629 \pm 1.48 \times 10^{-04}$. These results are consistent with those obtained using the R-function approach discussed above. Furthermore, by fitting the slope of $\log(L)$ versus $\log(\sigma_L)$, we derive the critical exponent ratios β/ν, which at the corresponding transition points are $\beta_1/\nu_1 = 0.2547 \pm 1.9 \times 10^{-05}$, $\beta_2/\nu_2 = 0.2447 \pm 2.5 \times 10^{-05}$, $\beta_3/\nu_3 = 0.3104 \pm 1.7 \times 10^{-05}$ and $\beta_4/\nu_4 = 0.3185 \pm 3.7 \times 10^{-05}$. Additionally, the obtained critical exponent ratios satisfy the hyperscaling law described by equation (12), $\frac{2\beta}{\nu} + \frac{\gamma}{\nu} = 1$.

5. Influence of inter-leg hopping

In this section, we separately examine the influence of inter-leg hopping on reentrant localization in the presence of staggered and uniform disorder. As illustrated in the schematic diagram in figure 1(b), the inter-leg hopping is defined by the parameters J_{11} and J_3. Using the parameters marked by dashed lines in figures 3(c) and 9(c), we investigate the effect of varying J_{11} and J_3, while maintaining $J_{11} = J_3$. The corresponding η-phase diagrams are shown in figure 15.

Figures 15(a) and (b) illustrate the case for staggered disorder. As the inter-leg hopping strength increases, the previously observed reentrant localization feature gradually diminishes, eventually completely disappearing at $J_{11} = J_3 = 0.207$. This behavior can be attributed to the competition between dimerized hopping and staggered disorder within each individual leg of the ladder. The inter-leg hopping weakens the effective dimerization strength, leading to the suppression of reentrant localization as inter-leg hopping increases.

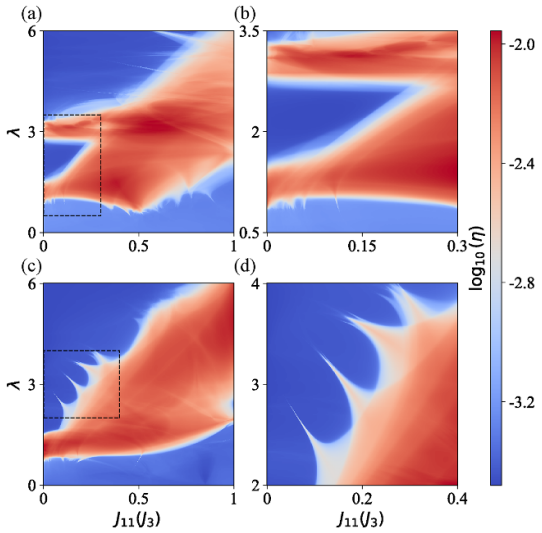

Figure 15. The η phase diagrams of the system in the disorder strength λ and inter-leg hopping $J_{11}(J_3)$ plane with (a) $J_{33}/J_1 = 2.7$ under staggered disorder and (c) $J_{33}/J_1 = 0.7$ under uniform disorder. (b) and (d) Present magnified views of the regions outlined by the dashed boxes in (a) and (c), respectively. All the phase diagrams are calculated under a system size $L = 3194$.

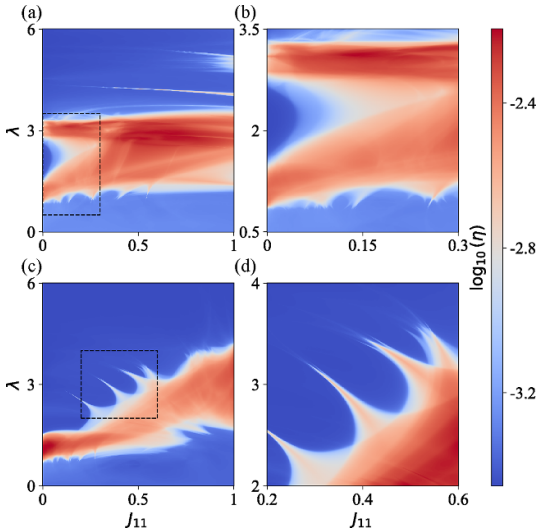

Figure 16. The η phase diagrams of the system in the disorder strength λ and inter-leg hopping J_{11} plane for (a) $J_{33}/J_1 = 2.7$ under staggered disorder and (c) $J_{33}/J_1 = 0.7$ under uniform disorder. (b) and (d) Present magnified views of the regions outlined by the dashed boxes in (a) and (c), respectively. All the phase diagrams are calculated under a system size $L = 3194$ and $J_3 = 0$.

For the case of uniform disorder, as shown in figures 15(c) and (d), reentrant localization does not initially appear at $J_{11} = J_3 = 0$. However, as the inter-leg hopping strength increases, the η-phase diagram begins to exhibit a 'spiky' structure similar to that observed in figure 9(c). These spikes indicate the emergence of reentrant localization transitions. With further increases in the inter-leg hopping strength, these spikes persist at various $J_{11} = J_3$ values but eventually vanish as the inter-leg hopping $J_{11}(J_3) > 0.35$. This demonstrates that, for uniform disorder, the appearance of reentrant localization requires a minimum of inter-leg hopping strength.

In figure 16, we examine the case where $J_3 = 0$, simplifying the ladder structure in figure 1 to one without slanted hopping. By calculating the η-phase diagrams, we also observe distinct behaviors under staggered and uniform disorder. For staggered disorder, the inter-leg hopping J_{11} progressively diminishes the originally observed reentrant localization phenomenon, consistent with our earlier findings that inter-leg hopping disrupts the competition between dimerized hopping and staggered disorder, which is crucial for reentrant localization. In contrast, for uniform disorder, the emergence of reentrant localization requires a non-zero inter-leg hopping J_{11}. However, once J_{11} exceeds 0.51, the reentrant localization phenomenon disappears. This suggests that while a moderate strength of inter-leg hopping is necessary to induce reentrant localization under uniform disorder, excessive inter-leg hopping ultimately suppresses this behavior. These

results highlight the crucial role of inter-leg hopping in shaping the localization properties of the system under different disorder conditions.

6. Conclusion

In conclusion, we have investigated the phenomenon of reentrant localization, which has previously been observed in systems without long-range hopping. Although long-range hopping is generally expected to disrupt reentrant localization, our results show that under specific parameter conditions, varying the strength of long-range hopping can induce a reentrant localization phase diagram, similar to that found in staggered SSH systems. We perform a detailed analysis of the observed reentrant localization phenomena, including the spatial distribution of eigenstates across lattice sites and the presence of multiple mobility edges. These features confirm that the system undergoes a genuine reentrant localization transition. Additionally, our calculation of critical exponents reveals that long-range hopping gives rise to four distinct localization transition points, each characterized by unique critical exponents. Previous studies have suggested that systems with uniform disorder and small inter-intra detuning do not exhibit reentrant localization. In contrast, our work demonstrates that long-range hopping can induce reentrant localization even in the presence of uniform disorder. Furthermore, we observe that the reemergent extended states are located near the highest and lowest eigenenergy, which contrasts with the typical behavior observed in staggered disorder systems, where extended states generally appear near the middle of the eigenenergy spectrum. Finally, we explore the critical exponents associated with these transitions. Our results indicate that the inclusion of long-range hopping leads to distinct critical exponents at all four transition points, highlighting the complex and unique nature of localization phenomena in systems with long-range interactions.

Data availability statement

All data that support the findings of this study are included within the article (and any supplementary files).

Acknowledgments

The authors thank Yuhang Lu for his helpful discussion. This work is supported by the National Natural Science Foundation of China under Grant Nos. 11974205, and 61727801, the Key Research and Development Program of Guangdong province (2018B030325002), and National Natural Science Foundation of China under Grant 62131002.

ORCID iD

Jinghui Pi https://orcid.org/0000-0002-6899-8132

References

[1] Anderson P W 1958 Absence of diffusion in certain random lattices *Phys. Rev.* **109** 1492
[2] Lee P A and Ramakrishnan T V 1985 Disordered electronic systems *Rev. Mod. Phys.* **57** 287
[3] Evers F and Mirlin A D 2008 Anderson transitions *Rev. Mod. Phys.* **80** 1355
[4] Roati G, D'Errico C, Fallani L, Fattori M, Fort C, Zaccanti M, Modugno G, Modugno M and Inguscio M 2008 Anderson localization of a non-interacting Bose–Einstein condensate *Nature* **453** 895
[5] Lahini Y, Pugatch R, Pozzi F, Sorel M, Morandotti R, Davidson N and Silberberg Y 2009 Observation of a localization transition in quasiperiodic photonic lattices *Phys. Rev. Lett.* **103** 013901
[6] Aspect A and Inguscio M 2009 Anderson localization of ultracold atoms *Phys. Today* **62** 30
[7] Kondov S, McGehee W, Zirbel J and DeMarco B 2011 Three-dimensional Anderson localization of ultracold matter *Science* **334** 66
[8] Jendrzejewski F, Bernard A, Mueller K, Cheinet P, Josse V, Piraud M, Pezzé L, Sanchez-Palencia L, Aspect A and Bouyer P 2012 Three-dimensional localization of ultracold atoms in an optical disordered potential *Nat. Phys.* **8** 398
[9] Semeghini G, Landini M, Castilho P, Roy S, Spagnolli G, Trenkwalder A, Fattori M, Inguscio M and Modugno G 2015 Measurement of the mobility edge for 3D Anderson localization *Nat. Phys.* **11** 554
[10] Pasek M, Orso G and Delande D 2017 Anderson localization of ultracold atoms: where is the mobility edge? *Phys. Rev. Lett.* **118** 170403
[11] Hainaut C, Rançon A, Clément J-F, Manai I, Szriftgiser P, Delande D, Garreau J C and Chicireanu R 2019 Experimental realization of an ideal floquet disordered system *New J. Phys.* **21** 035008
[12] Richard J *et al* 2019 Elastic scattering time of matter waves in disordered potentials *Phys. Rev. Lett.* **122** 100403
[13] Maynard J D 2001 Acoustical analogs of condensed-matter problems *Rev. Mod. Phys.* **73** 401
[14] Ye Y, Ke M, Feng J, Wang M, Qiu C and Liu Z 2015 Transversal Anderson localization of sound in acoustic waveguide arrays *J. Phys.: Condens. Matter* **27** 155402
[15] Hu H, Strybulevych A, Page J, Skipetrov S E and van Tiggelen B A 2008 Localization of ultrasound in a three-dimensional elastic network *Nat. Phys.* **4** 945
[16] Yamilov A, Skipetrov S E, Hughes T W, Minkov M, Yu Z and Cao H 2023 Anderson localization of electromagnetic waves in three dimensions *Nat. Phys.* **19** 1308

[17] Segev M, Silberberg Y and Christodoulides D N 2013 Anderson localization of light *Nat. Photon.* **7** 197
[18] Mookherjea S, Ong J R, Luo X and Guo-Qiang L 2014 Electronic control of optical Anderson localization modes *Nat. Nanotechnol.* **9** 365
[19] Vatnik I D, Tikan A, Onishchukov G, Churkin D V and Sukhorukov A A 2017 Anderson localization in synthetic photonic lattices *Sci. Rep.* **7** 4301
[20] Lahini Y, Avidan A, Pozzi F, Sorel M, Morandotti R, Christodoulides D N and Silberberg Y 2008 Anderson localization and nonlinearity in one-dimensional disordered photonic lattices *Phys. Rev. Lett.* **100** 013906
[21] Kovács T G and Pittler F 2010 Anderson localization in quark-gluon plasma *Phys. Rev. Lett.* **105** 192001
[22] Ghasempour Ardakani A, Mahboudi Z and Golshani M 2023 Anderson localization in disordered multilayered structures composed of plasma layers with modulated sinusoidal densities *Phys. Plasmas* **30** 072102
[23] Crespi A, Osellame R, Ramponi R, Giovannetti V, Fazio R, Sansoni L, De Nicola F, Sciarrino F and Mataloni P 2013 Anderson localization of entangled photons in an integrated quantum walk *Nat. Photon.* **7** 322
[24] Chen Y *et al* 2014 Emulating weak localization using a solid-state quantum circuit *Nat. Commun.* **5** 5184
[25] Ghosh J 2014 Simulating Anderson localization via a quantum walk on a one-dimensional lattice of superconducting qubits *Phys. Rev. A* **89** 022309
[26] Abrahams E, Anderson P W, Licciardello D C and Ramakrishnan T V 1979 Scaling theory of localization: absence of quantum diffusion in two dimensions *Phys. Rev. Lett.* **42** 673
[27] Serge Aubry G A 1980 Analyticity breaking and Anderson localization in incommensurate lattices *Ann. Isr. Phys. Soc.* **3** 133 (available at: https://www.researchgate.net/publication/265502988_Analyticity_breaking_and_Anderson_localization_in_incommensurate_lattices)
[28] Harper P G 1955 Single band motion of conduction electrons in a uniform magnetic field *Proc. Phys. Soc. A* **68** 874
[29] Kraus Y E, Lahini Y, Ringel Z, Verbin M and Zilberberg O 2012 Topological states and adiabatic pumping in quasicrystals *Phys. Rev. Lett.* **109** 106402
[30] Xue P, Qin H, Tang B and Sanders B C 2014 Observation of quasiperiodic dynamics in a one-dimensional quantum walk of single photons in space *New J. Phys.* **16** 053009
[31] Kim K, Chang M-S, Korenblit S, Islam R, Edwards E E, Freericks J K, Lin G-D, Duan L-M and Monroe C 2010 Quantum simulation of frustrated Ising spins with trapped ions *Nature* **465** 590
[32] Richerme P, Gong Z-X, Lee A, Senko C, Smith J, Foss-Feig M, Michalakis S, Gorshkov A V and Monroe C 2014 Non-local propagation of correlations in long-range interacting quantum systems *Nature* **511** 198–201
[33] Britton J W, Sawyer B C, Keith A C, Wang C-C J, Freericks J K, Uys H, Biercuk M J and Bollinger J J 2012 Engineered two-dimensional Ising interactions in a trapped-ion quantum simulator with hundreds of spins *Nature* **484** 489
[34] Islam R, Senko C, Campbell W C, Korenblit S, Smith J, Lee A, Edwards E, Wang C-C, Freericks J and Monroe C 2013 Emergence and frustration of magnetism with variable-range interactions in a quantum simulator *Science* **340** 583
[35] Schauß P, Zeiher J, Fukuhara T, Hild S, Cheneau M, Macrì T, Pohl T, Bloch I and Groß C 2015 Crystallization in Ising quantum magnets *Science* **347** 1455
[36] Baier S, Petter D, Becher J H, Patscheider A, Natale G, Chomaz L, Mark M J and Ferlaino F 2018 Realization of a strongly interacting Fermi gas of dipolar atoms *Phys. Rev. Lett.* **121** 093602
[37] Roy N and Sharma A 2021 Fraction of delocalized eigenstates in the long-range Aubry–André–Harper model *Phys. Rev. B* **103** 075124
[38] Roy N and Sharma A 2021 Entanglement entropy and out-of-time-order correlator in the long-range Aubry–André–Harper model *J. Phys.: Condens. Matter* **33** 334001
[39] Gandhi S and Bandyopadhyay J N 2024 Non-Hermitian Aubry–André–Harper model with short- and long-range *p*-wave pairing *Phys. Rev. B* **110** 094203
[40] Fraxanet J, Bhattacharya U, Grass T, Rakshit D, Lewenstein M and Dauphin A 2021 Topological properties of the long-range Kitaev chain with Aubry–André–Harper modulation *Phys. Rev. Res.* **3** 013148
[41] Wang Y, Xia X, Zhang L, Yao H, Chen S, You J, Zhou Q and Liu X-J 2020 One-dimensional quasiperiodic mosaic lattice with exact mobility edges *Phys. Rev. Lett.* **125** 196604
[42] Zhao J, Zhao Y, Wang J-G, Li Y and Bai X-D 2023 Phase transition of a non-Abelian quasiperiodic mosaic lattice model with *p*-wave superfluidity *Phys. Rev. B* **108** 054204
[43] Zeng Q-B and Lü R 2021 Topological phases and Anderson localization in off-diagonal mosaic lattices *Phys. Rev. B* **104** 064203
[44] Biddle J and Das Sarma S 2010 Predicted mobility edges in one-dimensional incommensurate optical lattices: an exactly solvable model of Anderson localization *Phys. Rev. Lett.* **104** 070601
[45] Ganeshan S, Pixley J H and Das Sarma S 2015 Nearest neighbor tight binding models with an exact mobility edge in one dimension *Phys. Rev. Lett.* **114** 146601
[46] Yao H, Khoudli A, Bresque L and Sanchez-Palencia L 2019 Critical behavior and fractality in shallow one-dimensional quasiperiodic potentials *Phys. Rev. Lett.* **123** 070405
[47] Roy S, Mishra T, Tanatar B and Basu S 2021 Reentrant localization transition in a quasiperiodic chain *Phys. Rev. Lett.* **126** 106803
[48] Zhou L and Han W 2022 Driving-induced multiple $\mathcal{PT}$-symmetry breaking transitions and reentrant localization transitions in non-Hermitian floquet quasicrystals *Phys. Rev. B* **106** 054307
[49] Han W and Zhou L 2022 Dimerization-induced mobility edges and multiple reentrant localization transitions in non-Hermitian quasicrystals *Phys. Rev. B* **105** 054204
[50] Gonçalves M, Amorim B, Castro E V and Ribeiro P 2023 Renormalization group theory of one-dimensional quasiperiodic lattice models with commensurate approximants *Phys. Rev. B* **108** L100201
[51] Padhan A, Giri M K, Mondal S and Mishra T 2022 Emergence of multiple localization transitions in a one-dimensional quasiperiodic lattice *Phys. Rev. B* **105** L220201
[52] Zuo Z-W and Kang D 2022 Reentrant localization transition in the Su–Schrieffer–Heeger model with random-dimer disorder *Phys. Rev. A* **106** 013305
[53] Wu C, Fan J, Chen G and Jia S 2021 Non-Hermiticity-induced reentrant localization in a quasiperiodic lattice *New J. Phys.* **23** 123048
[54] Li S-Z, Cheng E, Zhu S-L and Li Z 2024 Asymmetric transfer matrix analysis of Lyapunov exponents in one-dimensional nonreciprocal quasicrystals *Phys. Rev. B* **110** 134203
[55] Qi R, Cao J and Jiang X-P 2023 Multiple localization transitions and novel quantum phases induced by a staggered on-site potential *Phys. Rev. B* **107** 224201

[56] Aditya S, Sengupta K and Sen D 2023 Periodically driven model with quasiperiodic potential and staggered hopping amplitudes: engineering of mobility gaps and multifractal states *Phys. Rev. B* **107** 035402
[57] Ganguly S, Sarkar S, Mondal K and Maiti S K 2024 Phenomenon of multiple reentrant localization in a double-stranded helix with transverse electric field *Sci. Rep.* **14** 3059
[58] Li S-Z and Li Z 2023 The multiple re-entrant localization in a phase-shift quasiperiodic chain (arXiv:2305.12321)
[59] Wang Y 2022 Mobility edges and critical regions in a periodically kicked incommensurate optical raman lattice *Phys. Rev. A* **106** 053312
[60] Giri M K, Paul B and Mishra T 2024 Flux-enhanced localization and reentrant delocalization in the quench dynamics of two interacting bosons on a Bose-Hubbard ladder *Phys. Rev. A* **109** 043308
[61] Lu Z, Zhang Y and Xu Z 2023 Robust topological Anderson insulator induced reentrant localization transition (arXiv:2306.06818)
[62] Miranda D A, Antão T V C and Peres N M R 2024 Mechanical Su–Schrieffer–Heeger quasicrystal: topology, localization and mobility edge *Phys. Rev. B* **109** 195427
[63] Tabanelli H, Castelnovo C and Štrkalj A 2024 Reentrant localization transitions and anomalous spectral properties in off-diagonal quasiperiodic systems *Phys. Rev. B* **110** 184208
[64] Sarkar S K, Ravisankar R, Mishra T, Muruganandam P and Mishra P K 2024 Signature of reentrant localization in collisional inhomogeneous spin-orbit coupled condensates (arXiv:2403.02027)
[65] Gong L, Lu H and Cheng W 2021 Comment on "Reentrant localization transition in a quasiperiodic chain" (arXiv:2106.07818)
[66] Padhan A, Padhi S R and Mishra T 2024 Complete delocalization and reentrant topological transition in a non-Hermitian quasiperiodic lattice *Phys. Rev. B* **109** L020203
[67] Guan E, Wang G, Guan X-W and Cai X 2023 Reentrant localization and mobility edges in a spinful Aubry–André–Harper model with a non-Abelian potential *Phys. Rev. A* **108** 033305
[68] Jiang X-P, Qiao Y and Cao J-P 2021 Mobility edges and reentrant localization in one-dimensional dimerized non-Hermitian quasiperiodic lattice *Chin. Phys. B* **30** 097202
[69] Wang H, Zheng X, Chen J, Xiao L, Jia S and Zhang L 2023 Fate of the reentrant localization phenomenon in the one-dimensional dimerized quasiperiodic chain with long-range hopping *Phys. Rev. B* **107** 075128
[70] Xu Z-S, Gao J, Iovan A, Khaymovich I M, Zwiller V and Elshaari A W 2024 Observation of reentrant metal-insulator transition in a random-dimer disordered SSH lattice *npj Nanophoton.* **1** 8
[71] Vaidya S, Jörg C, Linn K, Goh M and Rechtsman M C 2023 Reentrant delocalization transition in one-dimensional photonic quasicrystals *Phys. Rev. Res.* **5** 033170
[72] Roy S, Chattopadhyay S, Mishra T and Basu S 2022 Critical analysis of the reentrant localization transition in a one-dimensional dimerized quasiperiodic lattice *Phys. Rev. B* **105** 214203
[73] Hashimoto Y, Niizeki K and Okabe Y 1992 A finite-size scaling analysis of the localization properties of one-dimensional quasiperiodic systems *J. Phys. A: Math. Gen.* **25** 5211
[74] Li X and Das Sarma S 2020 Mobility edge and intermediate phase in one-dimensional incommensurate lattice potentials *Phys. Rev. B* **101** 064203
[75] Pérez-González B, Bello M, Gómez-León A and Platero G 2018 SSH model with long-range hoppings: topology, driving and disorder (arXiv:1802.03973)
[76] Pérez-González B, Bello M, Gómez-León A and Platero G 2019 Interplay between long-range hopping and disorder in topological systems *Phys. Rev. B* **99** 035146